

VR-Goggles for Robots: Real-to-sim Domain Adaptation for Visual Control

Jingwei Zhang^{*†}Lei Tai^{*‡}Yufeng Xiong[†]Peng Yun[‡]Ming Liu[‡]Joschka Boedecker[†]Wolfram Burgard[†]

Abstract: In this paper, we deal with the *reality gap* from a novel perspective, targeting transferring Deep Reinforcement Learning (DRL) policies learned in simulated environments to the real-world domain for visual control tasks. Instead of adopting the common solutions to the problem by increasing the visual fidelity of synthetic images output from simulators during the training phase, we seek to tackle the problem by translating the real-world image streams back to the synthetic domain during the deployment phase, to *make the robot feel at home*. We propose this as a lightweight, flexible, and efficient solution for visual control, as 1) no extra transfer steps are required during the expensive training of DRL agents in simulation; 2) the trained DRL agents will not be constrained to being deployable in only one specific real-world environment; 3) the policy training and the transfer operations are decoupled, and can be conducted in parallel. Besides this, we propose a simple yet effective *shift loss* to constrain the consistency between subsequent frames, which is important for consistent policy outputs. We validate the *shift loss* for *artistic style transfer for videos* and *domain adaptation*, and validate our visual control approach in both indoor and outdoor robotics experiments. A video of our results is available at: <https://goo.gl/P76TTo>.

Keywords: domain adaptation, deep reinforcement learning, real-to-sim

1 Introduction

Pioneered by the Deep Q-network [1] and followed up by various extensions and advancements [2, 3, 4, 5], Deep Reinforcement Learning (DRL) algorithms show great potential in solving high-dimensional real-world robotics sensory control tasks. However, DRL methods typically require several millions of training samples, making them infeasible to train directly on real robotic systems. As a result, DRL algorithms are generally trained in simulated environments, then transferred to and deployed in real scenes. However, the *reality gap*, namely the noise pattern, texture, lighting condition discrepancies, etc., between synthetic renderings and real sensory readings, imposes major challenges for generalizing the sensory control policies trained in simulation to reality.

In this paper, we focus on visual control tasks, where autonomous agents perceive the environment with their onboard cameras, and execute commands based on the color image reading streams. A natural way and also the typical choice in the recent literature on dealing with the *reality gap* for visual control, is by increasing the visual fidelity of the simulated images [6], by matching the distribution of synthetic images to that of the real ones [7], and by gradually adapting the learned features and representations from the simulated domain to the real-world domain [8]. These *sim-to-real* methods, however, inevitably have to add preprocessing steps for each individual training frame to the already expensive learning pipeline of DRL control policies; also, the complete policy

^{*}indicates equal contribution.

[†]Jingwei Zhang, Yufeng Xiong, Joschka Boedecker and Wolfram Burgard are with the University of Freiburg. {zhang, xiongy, jboedeck, burgard}@cs.uni-freiburg.de

[‡]Lei Tai, Peng Yun and Ming Liu are with the Hong Kong University of Science and Technology. {ltai, pyun, celiu}@ust.hk

training phase has to be conducted again for each visually different real-world scene. Attempts for more realistic simulation renderings often adds to the computational burden.

This paper attempts to tackle the *reality gap* in the visual control domain from a novel perspective, with the aim of adding minimal extra computational burden to the learning pipeline. We cope with the *reality gap* only during the actual deployment phase of agents in real-world scenario, by adapting the real camera streams to the synthetic modality, so as to translate the unfamiliar or unseen features of real images back into the simulated style, which the agents have already learned how to deal with during training in simulation.

Compared to other *sim-to-real* methods bridging the *reality gap*, our proposed *real-to-sim* approach, which we refer to as the *VR-Goggles*, has several appealing properties: (1) Our proposed method is highly lightweight: It does not add any extra processing burden to the training phase of DRL policies; (2) Our approach is highly flexible and efficient: Since we decouple the policy training and the adaptation operations, the preparations for transferring the policies from simulation to the real world can be conducted in parallel with the training of the control policies. From each visually different real-world environment that we expect to deploy the agent in, we just need to collect several (typically on the order of 2000) images, and train a *VR-Goggles* model for each of them. More importantly, we do not need to retrain or finetune the visual control policy for new environments.

As an additional contribution, we propose a new *shift loss*, which enables generating consistent synthetic image streams without imposing temporal constraints, or even sequential training data. We show that *shift loss* is a promising and cheap alternative to the constraints imposed by optical flow, and demonstrate its effectiveness in *artistic style transfer for videos* and *domain adaptation*.

2 Related Works

2.1 Domain Adaptation

Domain adaptation, also referred to as *image-to-image translation*, targets translating images from a source domain into a target domain. We here focus on the most general unsupervised methods that require the least manual effort and are applicable in robotics control tasks.

CycleGAN [9] introduced a cycle-consistent loss to enforce an inverse mapping from the target domain to the source domain on top of the source to target mapping. It does not require paired data from the two domains of interest and shows convincing results for relatively simple data distributions containing few semantic types. However, in terms of translating between more complex data distributions containing many more semantic types, its results are not as satisfactory, in that permutations of semantics often occur. *CyCADA* [10] added a semantic constraint on top, to enforce a match between the semantic map of the translated image and that of the input. However, the semantic loss was not added in its experiments on large datasets due to memory limitations.

Following the observation that several most recent and advanced robotics simulators do provide semantic ground truth, and the semantic segmentation literature is quite mature (e.g., [11]), we adopt the semantic constraint from *CyCADA* into our method. We are able to include the semantic loss calculation with special configurations (Appendix C).

2.2 Domain Adaptation for DRL

DRL has been applied to robotics control tasks such as manipulation and navigation. Below, we review the recent literature with an emphasis on works considering the *reality gap*.

For manipulation, Bousmalis et al. [6] bridged the *reality gap* by adapting synthetic images to the realistic domain during training. However, the addition of an adaptation step before every training iteration can greatly slow down the whole learning pipeline. Tobin et al. [7] proposed to randomize the texture of objects, lighting conditions, and camera positions during training, such that the learned model could generalize naturally to real-world scenarios. However, such randomization could not be easily satisfied at a low cost by most of the popular robotic simulators. Moreover, there is no guarantee that these randomized simulations can cover the visual modality of a random real-world scene. Rusu et al. [8] deals with the *reality gap* by progressively adapting the features and representations learned in simulation to that of the realistic domain. This method, however, still needs to go through an expensive control policy training phase for each visually different real-world scenario.

For navigation, where autonomous agents are expected to encounter sensor readings of environments at a much larger scale than manipulation in terms of visual inputs, the *reality gap* has not been directly dealt with in the literature of learning-based visual control to the best of our knowledge. Some works, however, chose special setups to circumvent the *reality gap*. For example, 2D Lidar [12, 13, 14] and depth images [15, 16] are sometimes chosen as the sensor modality for transferring the navigation policies to the real world, since the discrepancies between the simulated domain and the real-world domain for them are smaller than those for color images. Zhu et al. [17] conducted real-world experiments with visual inputs. However, in their setups, the real-world scene is highly visually similar to their simulation, a condition that can rarely be met in practice.

In this paper, we mainly consider *domain adaptation* for learning-based visual navigation, which has not yet been considered in the literature. We believe the adaptation for navigation is much more challenging than for manipulation, since navigation agents usually work in environments at much larger scales with more complexities in terms of visual features than the confined workspace for manipulators. We believe our proposed *real-to-sim* method can be naturally adopted in manipulation.

An important aspect of *domain adaptation*, within the context of dealing with the *reality gap*, is the consistency between subsequent frames, which has not yet been considered in any of the aforementioned adaptation methods. As an approach for solving sequential decision making, the consistency between the subsequent inputs for DRL agents can be critical for the successful fulfillment of their final goals. Apart from the solutions for solving the *reality gap*, the general *domain adaptation* literature also lacks works considering sequential frames instead of single frames. Therefore, we look to borrow techniques from other fields that successfully extend single-frame algorithms to the video domain, among which the most applicable methods are from the *artistic style transfer* literature.

2.3 Artistic Style Transfer for Videos

Artistic style transfer is a technique for transferring the artistic style of artworks to photographs [18]. *Artistic style transfer for videos* works on video sequences instead of individual frames, targeting generating temporally consistent stylizations for sequential inputs. Ruder et al. [19] provides a key observation that: a trained stylization network with a total downsampling factor of s (e.g., $s = 4$ for a network with 2 convolutional layers of stride 2), is shift invariant to shifts equal to the multiples of s pixels, but can output significantly different stylizations otherwise. This undesired property (of not being shift invariant) causes the output of the trained network to change significantly for even very small changes in the input, which leads to temporal inconsistency (under the assumption that only relatively limited changes would appear in subsequent input frames). However, their solution of adding temporal constraints between generated subsequent frames, is rather expensive, as it requires optical flow as input during deployment. Huang et al. [20] offers a relatively cheap solution, requiring the temporal constraint only during training single-frame *artistic style transfer*. However, we believe that constraining optical flow on single frames is not well-defined. We suspect that their improved temporal consistency is actually due to the inexplicitly imposed consistency constraints for regional shifts by optical flow. We validate this suspicion in our experiments (Sec. 4.1).

We believe that the fundamental problem causing the inconsistency can be solved by an additional constraint of *shift loss*, which we introduce in Sec. 3.4. We show that the *shift loss* constrains the consistency between generated subsequent frames, without the need for the relatively expensive optical flow constraint. We argue that for a network that has been properly trained to learn a smooth function approximation, small changes in the input should also result in small changes in the output.

3 Methods

3.1 Problem formulation

We consider visual data sources from two domains: \mathbf{X} , containing sequential frames $\{\mathbf{x}_0, \mathbf{x}_1, \mathbf{x}_2, \dots\}$ (e.g., synthetic images output from a simulator; $\mathbf{x} \sim p_{\text{sim}}$, where p_{sim} denotes the simulated data distribution), and \mathbf{Y} , containing sequential frames $\{\mathbf{y}_0, \mathbf{y}_1, \mathbf{y}_2, \dots\}$ (e.g., real camera readings from the onboard camera of a mobile robot; $\mathbf{y} \sim p_{\text{real}}$, where p_{real} denotes the distribution of the real sensory readings). We emphasize that, although we require our method to generate consistent outputs for sequential inputs, we do not need the training data to be sequential; we formalize it in this way only because some of our baseline methods have this requirement.

DRL agents are typically trained in the simulated domain \mathbf{X} , and expected to execute in the real-world domain \mathbf{Y} . As we have discussed, we choose to tackle this problem by translating the images from \mathbf{Y} to \mathbf{X} during deployment. In the following we introduce our approach for performing *domain adaptation*. Also to cope with the sequential nature of the incoming data streams, we introduce a *shift loss* technique for constraining the consistency of the translated subsequent frames.

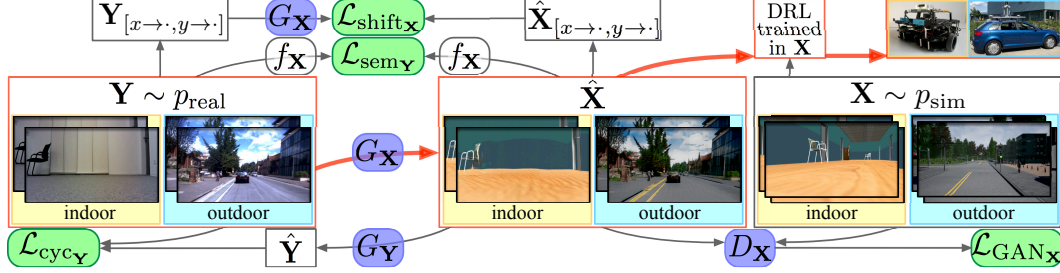


Figure 1: The VR-Goggles pipeline. We depict the computation of the losses $\mathcal{L}_{\text{GAN}_\mathbf{X}}$, $\mathcal{L}_{\text{cyc}_\mathbf{Y}}$, $\mathcal{L}_{\text{sem}_\mathbf{Y}}$ and $\mathcal{L}_{\text{shift}_\mathbf{X}}$. We present both *outdoor* and *indoor* scenarios, where the adaptation for the *outdoor* scene is trained with the semantic loss \mathcal{L}_{sem} (since its simulated domain *CARLA* has ground truth semantic labels to train a segmentation network $f_\mathbf{X}$), and the *indoor* one without (since its simulated domain *Gazebo* does not provide semantic ground truth). The components marked in red are those involved in the final deployment: a real sensor reading is captured ($\mathbf{y} \sim p_{\text{real}}$), then passed through the generator $G_\mathbf{X}$ to be translated into the simulated domain \mathbf{X} , where the DRL agents were originally trained; the translated image $\hat{\mathbf{x}}$ is then fed to the DRL policy, which outputs control commands. For clarity, we skip the counterpart losses $\mathcal{L}_{\text{GAN}_\mathbf{Y}}$, $\mathcal{L}_{\text{cyc}_\mathbf{X}}$, $\mathcal{L}_{\text{sem}_\mathbf{X}}$ and $\mathcal{L}_{\text{shift}_\mathbf{Y}}$.

3.2 CycleGAN Loss

To achieve this, we first build on top of *CycleGAN* [9], which learns two generative models to map between domains: $G_\mathbf{Y} : \mathbf{X} \rightarrow \mathbf{Y}$, with its discriminator $D_\mathbf{Y}$, and $G_\mathbf{X} : \mathbf{Y} \rightarrow \mathbf{X}$, with its discriminator $D_\mathbf{X}$, via training two GANs simultaneously:

$$\mathcal{L}_{\text{GAN}_\mathbf{Y}}(G_\mathbf{Y}, D_\mathbf{Y}; \mathbf{X}, \mathbf{Y}) = \mathbb{E}_\mathbf{Y} [\log D_\mathbf{Y}(\mathbf{y})] + \mathbb{E}_\mathbf{X} [\log(1 - D_\mathbf{Y}(G_\mathbf{Y}(\mathbf{x})))] , \quad (1)$$

$$\mathcal{L}_{\text{GAN}_\mathbf{X}}(G_\mathbf{X}, D_\mathbf{X}; \mathbf{Y}, \mathbf{X}) = \mathbb{E}_\mathbf{X} [\log D_\mathbf{X}(\mathbf{x})] + \mathbb{E}_\mathbf{Y} [\log(1 - D_\mathbf{X}(G_\mathbf{X}(\mathbf{y})))] , \quad (2)$$

in which $G_\mathbf{Y}$ learns to generate images $G_\mathbf{Y}(\mathbf{x})$ matching those from domain \mathbf{Y} , while $G_\mathbf{X}$ tries translating \mathbf{y} to domain \mathbf{X} . We also constrain those mappings with the *cycle consistency loss* [9]:

$$\mathcal{L}_{\text{cyc}_\mathbf{Y}}(G_\mathbf{X}, G_\mathbf{Y}; \mathbf{Y}) = \mathbb{E}_\mathbf{Y} [\|G_\mathbf{Y}(G_\mathbf{X}(\mathbf{y})) - \mathbf{y}\|_1] , \quad (3)$$

$$\mathcal{L}_{\text{cyc}_\mathbf{X}}(G_\mathbf{Y}, G_\mathbf{X}; \mathbf{X}) = \mathbb{E}_\mathbf{X} [\|G_\mathbf{X}(G_\mathbf{Y}(\mathbf{x})) - \mathbf{x}\|_1] . \quad (4)$$

3.3 Semantic Loss

Since our translation domains of interest are between synthetic images and real-world sensor images, we take advantage of the fact that many recent robotic simulators provide ground truth semantic labels and add a semantic constraint inspired by *CyCADA* [10].

Assuming that for images from domain \mathbf{X} , the ground truth semantic information $S_\mathbf{X}$ is available, a semantic segmentation network $f_\mathbf{X}$ can be easily obtained by minimizing the *cross-entropy* loss, denoted $\text{CrossEnt}(S_\mathbf{X}, f_\mathbf{X}(\mathbf{X}))$. We further assume that the ground truth semantic for domain \mathbf{Y} is lacking (which is the case for most real scenarios), meaning that $f_\mathbf{Y}$ is not easily accessible. In this case, we provide "semi" semantic supervision to the training agents: After $f_\mathbf{X}$ for semantic segmentation of domain \mathbf{X} is obtained, "semi" semantic supervision for the generators can be incorporated, by imposing consistency between the semantic map of the input and that of the generated output. This semantically consistent image translation can be achieved by minimizing the following losses (we use $f_\mathbf{X}$ also to generate "semi" semantic labels for domain \mathbf{Y}):

$$\mathcal{L}_{\text{sem}_\mathbf{Y}}(G_\mathbf{Y}; \mathbf{X}, f_\mathbf{X}) = \text{CrossEnt}(f_\mathbf{X}(\mathbf{X}), f_\mathbf{X}(G_\mathbf{Y}(\mathbf{X}))), \quad (5)$$

$$\mathcal{L}_{\text{sem}_\mathbf{X}}(G_\mathbf{X}; \mathbf{Y}, f_\mathbf{X}) = \text{CrossEnt}(f_\mathbf{X}(\mathbf{Y}), f_\mathbf{X}(G_\mathbf{X}(\mathbf{Y}))). \quad (6)$$

3.4 Shift Loss for Consistent Generation

Different from the current literature of *domain adaptation*, our model is additionally expected to output consistent images for sequential inputs. Although with \mathcal{L}_{sem} , the semantics of the consecutive outputs are constrained, inconsistencies and artifacts still occur quite often. Moreover, in cases where ground truth semantics are unavailable from either domain, the sequential outputs are even less constrained, which could potentially lead to inconsistent DRL policy outputs. Following the discussions in Sec. 2.3, we introduce the *shift loss* to constrain the consistency even in these situations.

For an input image \mathbf{x} , we use $\mathbf{x}_{[x \rightarrow i, y \rightarrow j]}$ to denote the result of a shift operation: shifting \mathbf{x} along the X axis by i pixels, and j pixels along the Y axis. We sometimes omit $y \rightarrow 0$ or $x \rightarrow 0$ in the subscript if the image is only shifted along the X or Y axis. According to [19], a trained stylization network is shift invariant to shifts of multiples of s pixels (s represents the total downsampling factor of the network), but can output significantly different stylizations otherwise. This causes the output of the trained network to change greatly for even very small changes in the input. We thus propose to add a conceptually simple yet direct and effective *shift loss* (u denotes the uniform distribution):

$$\mathcal{L}_{\text{shift}_Y}(G_Y; \mathbf{X}) = \mathbb{E}_{\mathbf{x}, i, j \sim u(1, s-1)} \left[\left\| G_Y(\mathbf{x})_{[x \rightarrow i, y \rightarrow j]} - G_Y(\mathbf{x}_{[x \rightarrow i, y \rightarrow j]}) \right\|_2^2 \right], \quad (7)$$

$$\mathcal{L}_{\text{shift}_X}(G_X; \mathbf{Y}) = \mathbb{E}_{\mathbf{y}, i, j \sim u(1, s-1)} \left[\left\| G_X(\mathbf{y})_{[x \rightarrow i, y \rightarrow j]} - G_X(\mathbf{y}_{[x \rightarrow i, y \rightarrow j]}) \right\|_2^2 \right]. \quad (8)$$

Shift loss constrains the shifted output to match the output of the shifted input, regarding the shifts as image-scale movements. Assuming that only limited regional movement would appear in subsequent input frames, *shift loss* effectively smoothes the mapping function for small regional movements, restricting the changes in its outputs for subsequent inputs. This can be regarded as a cheap alternative for imposing consistency constraints on small movements, eliminating the need for the optical flow information, which is crucial for meeting the requirement of real-time robotics control.

3.5 Full Objective

Our full objective for learning *VR-Goggles* (Fig. 1) is (λ_{cyc} , λ_{sem} and λ_{shift} are the loss weightings):

$$\begin{aligned} \mathcal{L}(G_Y, G_X, D_Y, D_X; \mathbf{X}, \mathbf{Y}, f_X) = & \mathcal{L}_{\text{GAN}_Y}(G_Y, D_Y; \mathbf{X}, \mathbf{Y}) + \mathcal{L}_{\text{GAN}_X}(G_X, D_X; \mathbf{Y}, \mathbf{X}) \\ & + \lambda_{\text{cyc}} (\mathcal{L}_{\text{cyc}_Y}(G_X, G_Y; \mathbf{Y}) + \mathcal{L}_{\text{cyc}_X}(G_Y, G_X; \mathbf{X})) \\ & + \lambda_{\text{sem}} (\mathcal{L}_{\text{sem}_Y}(G_Y; \mathbf{X}, f_X) + \mathcal{L}_{\text{sem}_X}(G_X; \mathbf{Y}, f_X)) \\ & + \lambda_{\text{shift}} (\mathcal{L}_{\text{shift}_Y}(G_Y; \mathbf{X}) + \mathcal{L}_{\text{shift}_X}(G_X; \mathbf{Y})). \end{aligned} \quad (9)$$

This corresponds to solving the following optimization:

$$G_Y^*, G_X^* = \arg \min_{G_Y, G_X} \max_{D_Y, D_X} \mathcal{L}(G_Y, G_X, D_Y, D_X). \quad (10)$$

4 Experiments

4.1 Validating Shift Loss: Artistic Style Transfer for Videos

To evaluate our method, we firstly conduct experiments for *artistic style transfer* for videos, to validate the effectiveness of *shift loss* on constraining consistency for sequential frames. We collect a training dataset of 98 HD video footage sequences (from *VIDEVO* [21] containing 2450 frames in total); the *Sintel* [22] sequences are used for testing, as their ground-truth optical flow is available. We compare the performance of the models trained under the following setups: (1) **FF** [18]: Canonical feed forward style transfer trained on single frames; (2) **FF+flow** [20]: *FF* trained on sequential images, with optical flow added for imposing temporal constraints on subsequent frames; (3) **Ours**: *FF* trained on single frames, with an additional *shift loss* as discussed in Sec. 3.4.

Implementation-wise, we use the pretrained *VGG-19* as the loss network, *relu2_2* as the content layer, *relu1_2*, *relu2_2*, *relu3_2* and *relu4_2* as the style layers. We set the weight for each loss as: $1e5$ for content, 2 for style, $1e-7$ for spatial regularization, 10 for optical flow, and 100 for shift. The downsampling factor s for the transformer network [18] is 4. Shifts are uniformly sampled from $[1, s - 1]$ for every training frame.

As a proof of concept, we begin our evaluation by comparing the three setups on their ability to generate shift invariant stylizations for shifted single frames. In particular, for each image \mathbf{x} in the testing dataset, we generate 4 more test images by shifting the original image along the X axis by 1, 2, 3, 4 pixels respectively, and pass all 5 frames (\mathbf{x} , $\mathbf{x}_{[x \rightarrow 1]}$, $\mathbf{x}_{[x \rightarrow 2]}$, $\mathbf{x}_{[x \rightarrow 3]}$, $\mathbf{x}_{[x \rightarrow 4]}$) through the trained network to examine the consistency of the generated images. The results shown in Fig. 2 validate the discussion from [19], since the stylizations for \mathbf{x} and $\mathbf{x}_{[x \rightarrow 4]}$ from FF are almost identical ($s = 4$ for the trained network), but differ significantly otherwise. FF -flow improves the invariance by a limited amount; *Ours* is capable of generating consistent stylizations for shifted input frames, with the *shift loss* directly reducing the shift variance.

We then evaluate the consistency of stylized sequential frames, computing the temporal loss using the ground truth optical flow for the *Sintel* sequences (Table 1). Although the temporal loss is part of the optimization objective of FF -flow, and our method does not have access to any optical flow information, *Ours* is still able to achieve lower temporal loss with the *shift loss* constraint.

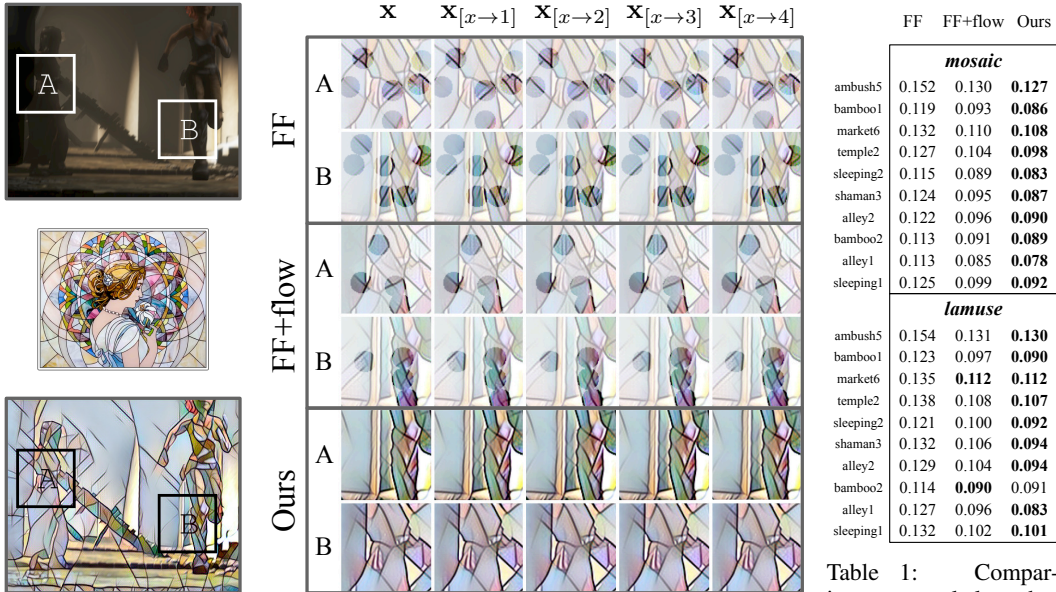


Figure 2: Shift-invariance evaluation, comparing between FF , FF +flow and *Ours*. We shift an input image \mathbf{x} along the X axis by 1, 2, 3, 4 pixels respectively and feed all 5 frames through the networks trained via FF , FF +flow and *Ours* and show the generated stylizations. We mark the most visible differences with small circles and dim the rest of the generated images. As is discussed in [19], FF generates almost identical stylizations for \mathbf{x} and $\mathbf{x}_{[x \rightarrow 4]}$ (because 4 is a multiple of the total down-sampling factor of the trained network), but those for $\mathbf{x}_{[x \rightarrow 1]}$, $\mathbf{x}_{[x \rightarrow 2]}$, $\mathbf{x}_{[x \rightarrow 3]}$ differ significantly. FF +flow improves the shift-invariance, but we suspect the improvement is due to the inexplicit consistency constraint on regional shifts imposed by optical flow. *Ours* generates shift-invariant stylizations with the proposed *shift loss*.

Table 1: Comparing temporal loss between FF , FF +flow and *Ours*. FF +flow directly optimizes on this metric, while optical flow is never provided to *Ours*; yet *Ours* achieves lower temporal loss on the evaluated *Sintel* sequences. See Appendix A for more results.

4.2 Comparing Policy Transfer Methods: Simulated Indoor Navigation

To illustrate the difference between the policy transfer pipelines of our proposed *real-to-sim* approach and several representative *sim-to-real* approaches discussed in Sec. 2.2, here we conduct a direct comparison in a simulated indoor navigation experiment.

We build an indoor office environment in *Gazebo* [23], and with two different sets of textures, we render two environments: *Sim-Env* and *Real-Env1*, shown on the right column of Fig. 3. We train agents to learn navigation policies to accomplish the task of navigating to chairs based purely on its front-facing color camera readings; the agent obtained a reward of -0.005 for a step cost, -0.05 for collision, and 1 for reaching the target. We illustrate the procedures of the following approaches to transfer policies learned in *Sim-Env* to *Real-Env1*, and show the average steps obtained by the agents in the evaluation during policy training in Fig. 3:

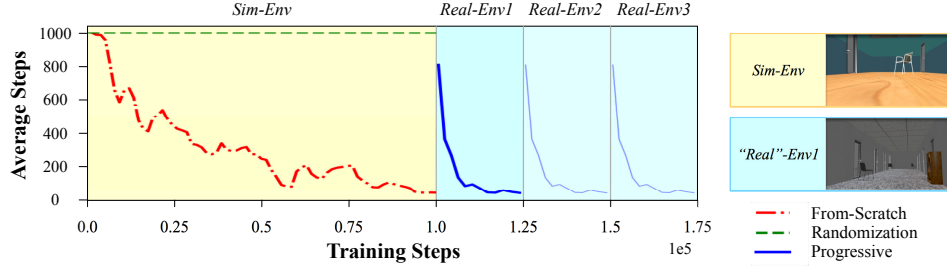


Figure 3: Average steps for completing episodes in evaluation during training, comparing policy transfer procedures of *From-Scratch*, *Randomization* and *Progressive*. We show median-filtered curves in line with [8].

(1) **From-Scratch** [2]: Canonical A3C trained from scratch on *Sim-Env*. We execute 8 training processes and 1 evaluation process, each with their own copy of *Sim-Env*. We note here that this is all the policy training required for our *real-to-sim* approach, as no fine-tuning or retraining of the policy is needed for deploying it in real-world scenes; also, since our approach decouples the policy training and the domain adaptation, the adaptation networks can be trained in parallel with the policy training. This is also the policy training procedure for several sim-to-real approaches such as [6], except that an additional adaptation step has to be added for each of the training frames; also, for each visually different real-world scene, this line of approaches needs to go through another complete policy training procedure. (2) **Randomization** (inspired by [7]): Our A3C variant of the *domain randomization* approach. *Domain randomization* [7] is initially presented on supervised learning problems (object detection), with the key concept of randomizing the textures, viewing angles, etc. of objects during the training in simulation, such that when deploying the trained model in real-world scenarios, the modality of the real-world objects could just be naturally dealt with as another variation. Here we adopt the same idea but implement it for our reinforcement learning task and under the constraints of our simulator (changing the texture for each frame is not as straightforward in *Gazebo*). In detail, each of the 8 training processes renders their environment with their own set of textures (all 8 sets of textures for the various objects in the environment are shown in Appendix B, Fig. 6). The evaluation process uses *Sim-Env* as its environment. We note here that this is all the policy training required for the *randomization* approach, since once converged, the agent is expected to be directly deployable in real-world environments. Unfortunately, for our considered task and setup, this approach does not manage to learn useful policies, as is shown by the green dashed line in Fig. 3 (we trained it for much longer iterations but still, it fails to converge). We suspect that different from the supervised learning task presented by Tobin et al. [7] where the supervision signal is strong and direct, with the sparse and delayed reward signals in our reinforcement learning task, the randomization might have imposed too many challenges for learning useful policies. (3) **Progressive** [8]: *Progressive Nets* for transferring the policy of *From-Scratch* on *Sim-Env* to “*Real*”-*Env1*. As described in [8], a second column is added after the first column is trained (the *From-Scratch* policy on *Sim-Env*). We note that for this approach, although the adaptation of the policy in new environments is significantly accelerated compared to training from scratch, the overall policy training needed contains both the initial training (the yellow block), and an adapting phase (the cyan blocks) in case we want to deploy the agent in new environments, e.g., *Real-Env2*, *Real-Env3*.

Having illustrated the advantage of our method in the *policy training* part, we continue to compare different approaches of implementing the *domain adaptation* part for our *real-to-sim* approach.

4.3 Comparing Domain Adaptation Methods: Real-world Indoor & Outdoor Navigation

We conduct real-world robotics experiments for both indoor and outdoor visual navigation tasks. We begin by training learning-based visual navigation policies, taking simulated first-person-view images as inputs, outputting moving commands for specific navigation targets. Then, we deploy the trained policy onto real robots, comparing the following *domain adaptation* approaches: (1) **No-Goggles**: Feed the sensor readings directly to the DRL policy; (2) **CycleGAN/CyCADA** [9, 10]: Use *CycleGAN* (when semantic ground truth is not available) / *CyCADA* (when ground truth semantic maps are provided by the simulator) to translate the real sensory inputs to the synthetic domain before feeding to policy nets; (3) **Ours**: Add *shift loss* on top of (2) as the **VR-Goggles**.

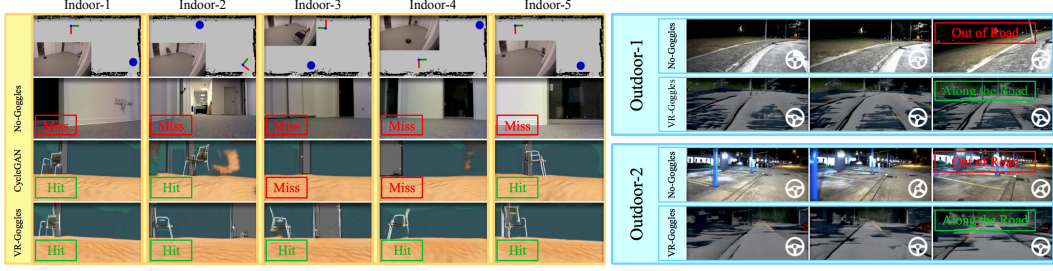


Figure 4: Real-world visual control experiments. **Indoor** (yellow): A navigation policy (*From-Scratch*, Sec. 4.2) is firstly trained in a simulated environment (*Sim-Env*, Fig. 3) that is able to navigate to chairs based on visual inputs. Without retraining or finetuning, our proposed *VR-Goggles* enables the mobile robot to directly deploy this policy in an office environment, achieving 100% success rate in a set of real-world experiments. Here *Miss* refers to test runs where the agent does not know what to do due to the *reality gap* or due to the unsatisfied quality of the translated image, or when it simply ignores the chair even when they are in sight; *Hit* refers to frames where the agent captures the chair in sight and outputs commands to move towards it. **Outdoor** (cyan): An autonomous driving policy (via conditional imitation learning [26]) is trained in *Carla* daytime, a *VR-Goggles* model is trained to translate between *Carla* daytime and *Robotcar* nighttime, which enables the real-world nighttime deployment of the trained policy. More details are presented in the attached video.

For **indoor** office experiments, $\mathbf{X} \sim p_{\text{sim}}$ are rendered from *Sim-Env* (Fig. 3) and $\mathbf{Y} \sim p_{\text{real}}$ are captured from a real office, using a *RealSense R200 camera* mounted on a *Turtlebot3 Waffle*. For conducting the *domain adaptation*, as the simulator (*Gazebo*) does not provide ground truth semantic labels, we drop the semantic constraint \mathcal{L}_{sem} . The input images are of size 640×360 , and the adaptation network is trained with 256×256 crops. We use the same network architecture as in *CycleGAN*, and train for 50 epochs with a learning rate of $2e - 4$, as we observe no performance gain training for longer iterations.

We deploy the trained policy of *From-Scratch* (Sec. 4.2) onto *Turtlebot3 Waffle* and compare the three *domain adaptation* approaches (Fig. 4). Without *domain adaptation*, *No-Goggles* fails completely in the real-world tasks; our proposed *VR-Goggles* achieves the highest success rate (0%, 60% and 100% for *No-Goggles*, *CycleGAN* and *Ours* respectively) due to the quality and consistency of the translated streams. The control cycle runs in real-time at 13Hz on a *Nvidia Jetson TX2*. Further experiment details can be found in the attached video, where we also show that the *VR-Goggles* can easily train a new model for a new type of chair without finetuning the control policy.

Finally, we conduct **outdoor** autonomous driving experiments ($\mathbf{X} \sim p_{\text{sim}}$ rendered from the *Carla* daytime [24] environment and $\mathbf{Y} \sim p_{\text{real}}$ sampled from a nighttime dataset of *Robotcar* [25]) with input images of size 640×400 . Considering that *VR-Goggles* outperforms *CycleGAN* in *indoor* experiments (also the additional *domain adaptation* experiments for *outdoor* scenes shown in Appendix C reach the same conclusion), and since outdoor robotics experiments are relatively expensive, we only compare *No-Goggles* and *VR-Goggles* in the *outdoor* autonomous driving scenario. We take the driving policy trained through conditional imitation learning [26] in the *Carla* environment as the baseline control method. This policy takes as inputs the first person view RGB image and a high-level command, which falls in a discrete action space and is generated through a global planner (*straight*, *left*, *right*, *follow*, *none*). In our real-world experiments, this high-level direction command is set as *straight*, indicating the vehicle (a *Bulldog* [27] with a *PointGrey Blackfly* camera mounted on it) to always go along the road. The output of the control policy is the steering angle.

The control policy is trained purely in a simulated daytime *Carla* environment, while we test the trained policy in a nighttime town way as shown in Fig. 4. It is non-trivial to quantitatively evaluate the control policy in the real world, so we show two representative subsequences of the input frames with the output steering commands represented by the steering wheel angles on it. The top row of the two scenarios presented are the continuous outputs of *No-Goggles*. Due to the huge difference between the real nighttime conditons and the simulated daytime environment, the vehicle failed to move along the road. Our *VR-Goggles* method, however, successfully guides the mobile vehicle to move along the road as instructed by the global planner (the policy prefers to turn right since it is trained in a right-driving environment). Further details are presented in the attached video.

5 Conclusions

In this paper, we tackled the *reality gap* occurring when deploying DRL visual control policies trained in simulation to the real world, by translating the real image streams back to the synthetic domain during deployment. Due to the sequential nature of the incoming sensor streams for control tasks, we propose *shift loss* to increase the consistency of the translated subsequent frames, and validate it both in *artistic style transfer for videos* and *domain adaptation*. We verify our proposed *VR-Goggles* pipeline as a lightweight, flexible and efficient solution for visual control through a set of real-world robotics experiments. It would be interesting to apply our method to manipulation, as we have been mainly focused on navigation in this paper. Also, evaluating our method in more challenging environments on more sophisticated control tasks could be another future direction.

References

- [1] V. Mnih, K. Kavukcuoglu, D. Silver, A. A. Rusu, J. Veness, M. G. Bellemare, A. Graves, M. Riedmiller, A. K. Fidjeland, G. Ostrovski, et al. Human-level control through deep reinforcement learning. *Nature*, 518(7540):529, 2015.
- [2] V. Mnih, A. P. Badia, M. Mirza, A. Graves, T. Lillicrap, T. Harley, D. Silver, and K. Kavukcuoglu. Asynchronous methods for deep reinforcement learning. In *International Conference on Machine Learning*, pages 1928–1937, 2016.
- [3] T. P. Lillicrap, J. J. Hunt, A. Pritzel, N. Heess, T. Erez, Y. Tassa, D. Silver, and D. Wierstra. Continuous control with deep reinforcement learning. *arXiv preprint arXiv:1509.02971*, 2015.
- [4] J. Schulman, S. Levine, P. Abbeel, M. Jordan, and P. Moritz. Trust region policy optimization. In *International Conference on Machine Learning*, pages 1889–1897, 2015.
- [5] J. Schulman, F. Wolski, P. Dhariwal, A. Radford, and O. Klimov. Proximal policy optimization algorithms. *arXiv preprint arXiv:1707.06347*, 2017.
- [6] K. Bousmalis, A. Irpan, P. Wohlhart, Y. Bai, M. Kelcey, M. Kalakrishnan, L. Downs, J. Ibarz, P. Pastor, K. Konolige, et al. Using simulation and domain adaptation to improve efficiency of deep robotic grasping. *arXiv preprint arXiv:1709.07857*, 2017.
- [7] J. Tobin, R. Fong, A. Ray, J. Schneider, W. Zaremba, and P. Abbeel. Domain randomization for transferring deep neural networks from simulation to the real world. In *Intelligent Robots and Systems (IROS), 2017 IEEE/RSJ International Conference on*, pages 23–30. IEEE, 2017.
- [8] A. A. Rusu, M. Večerík, T. Rothörl, N. Heess, R. Pascanu, and R. Hadsell. Sim-to-real robot learning from pixels with progressive nets. In *Conference on Robot Learning*, pages 262–270, 2017.
- [9] J.-Y. Zhu, T. Park, P. Isola, and A. A. Efros. Unpaired image-to-image translation using cycle-consistent adversarial networks. In *Proceedings of the IEEE Conference on Computer Vision and Pattern Recognition*, pages 2223–2232, 2017.
- [10] J. Hoffman, E. Tzeng, T. Park, J.-Y. Zhu, P. Isola, K. Saenko, A. A. Efros, and T. Darrell. Cycada: Cycle-consistent adversarial domain adaptation. *arXiv preprint arXiv:1711.03213*, 2017.
- [11] L. Chen, G. Papandreou, I. Kokkinos, K. Murphy, and A. Yuille. Deeplab: Semantic image segmentation with deep convolutional nets, atrous convolution, and fully connected crfs. *IEEE transactions on pattern analysis and machine intelligence*, 2017.
- [12] L. Tai, G. Paolo, and M. Liu. Virtual-to-real deep reinforcement learning: Continuous control of mobile robots for mapless navigation. In *2017 IEEE/RSJ International Conference on Intelligent Robots and Systems (IROS)*, pages 31–36, Sept 2017.
- [13] J. Zhang, L. Tai, J. Boedecker, W. Burgard, and M. Liu. Neural slam. *arxiv preprint arXiv:1706.09520*, 3, 2017.

- [14] O. Zhelo, J. Zhang, L. Tai, M. Liu, and W. Burgard. Curiosity-driven exploration for mapless navigation with deep reinforcement learning. *arXiv preprint arXiv:1804.00456*, 2018.
- [15] J. Zhang, J. T. Springenberg, J. Boedecker, and W. Burgard. Deep reinforcement learning with successor features for navigation across similar environments. In *2017 IEEE/RSJ International Conference on Intelligent Robots and Systems (IROS)*, pages 2371–2378, Sept 2017.
- [16] L. Tai, J. Zhang, M. Liu, and W. Burgard. Socially-compliant navigation through raw depth inputs with generative adversarial imitation learning. In *Robotics and Automation (ICRA), 2018 IEEE International Conference on*, May 2018.
- [17] Y. Zhu, R. Mottaghi, E. Kolve, J. J. Lim, A. Gupta, L. Fei-Fei, and A. Farhadi. Target-driven visual navigation in indoor scenes using deep reinforcement learning. In *Robotics and Automation (ICRA), 2017 IEEE International Conference on*, pages 3357–3364. IEEE, 2017.
- [18] J. Johnson, A. Alahi, and L. Fei-Fei. Perceptual losses for real-time style transfer and super-resolution. In *European Conference on Computer Vision*, pages 694–711. Springer, 2016.
- [19] M. Ruder, A. Dosovitskiy, and T. Brox. Artistic style transfer for videos and spherical images. *arXiv preprint arXiv:1708.04538*, 2017.
- [20] H. Huang, H. Wang, W. Luo, L. Ma, W. Jiang, X. Zhu, Z. Li, and W. Liu. Real-time neural style transfer for videos. In *Proceedings of the IEEE Conference on Computer Vision and Pattern Recognition*, pages 783–791, 2017.
- [21] Videvo. Videvo free footage. <http://www.videvo.net>, 2016.
- [22] D. J. Butler, J. Wulff, G. B. Stanley, and M. J. Black. A naturalistic open source movie for optical flow evaluation. In *European Conference on Computer Vision*, pages 611–625. Springer, 2012.
- [23] N. Koenig, B. A. and A. Howard. Design and use paradigms for gazebo, an open-source multi-robot simulator. In *Intelligent Robots and Systems, 2004.(IROS 2004). Proceedings. 2004 IEEE/RSJ International Conference on*, volume 3, pages 2149–2154. IEEE, 2004.
- [24] A. Dosovitskiy, G. Ros, F. Codevilla, A. Lopez, and V. Koltun. CARLA: An open urban driving simulator. In *Proceedings of the 1st Annual Conference on Robot Learning*, pages 1–16, 2017.
- [25] W. Maddern, G. Pascoe, C. Linegar, and P. Newman. 1 Year, 1000km: The Oxford RobotCar Dataset. *The International Journal of Robotics Research (IJRR)*, 36(1):3–15, 2017. doi:10.1177/0278364916679498. URL <http://dx.doi.org/10.1177/0278364916679498>.
- [26] F. Codevilla, M. Müller, A. López, V. Koltun, and A. Dosovitskiy. End-to-end driving via conditional imitation learning. In *International Conference on Robotics and Automation (ICRA)*, 2018.
- [27] Bulldog. Ros robots: Bulldog. <https://robots.ros.org/bulldog/>.
- [28] A. Dosovitskiy, G. Ros, F. Codevilla, A. Lopez, and V. Koltun. Carla: An open urban driving simulator. In *Conference on Robot Learning*, pages 1–16, 2017.

A Validating Shift Loss: Additional Materials

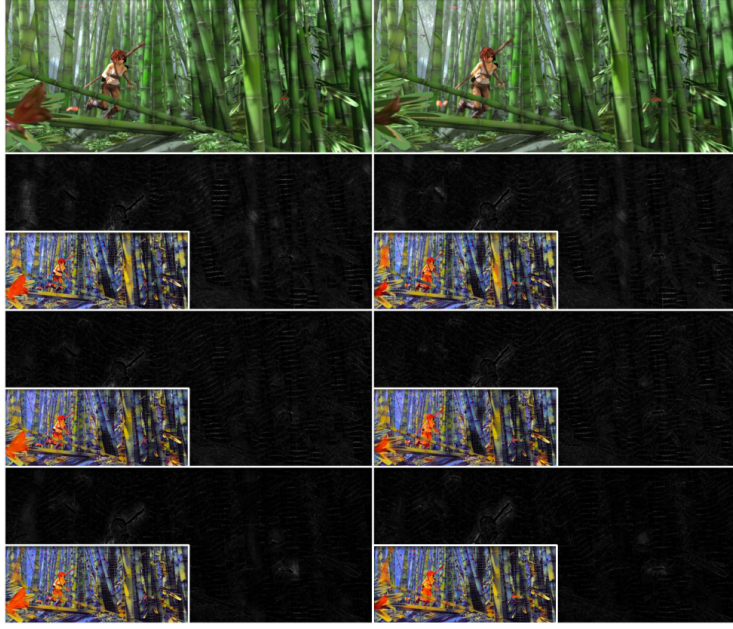


Figure 5: *Temporal error maps* between generated stylizations for subsequence input frames. 1st row: input frames; 2nd ~ 4th row: temporal error maps (with the corresponding stylizations shown on top) of outputs from *FF*, *FF+flow*, and *Ours*. We here choose a very challenging style (*mosaic*) for temporal consistency, as it contains many fine details, with tiny tiles laid over the original image in the final stylizations. Yet, *Ours* achieves very high consistency.

We conduct additional experiments for evaluating the consistency of the stylized sequential input frames. In Fig. 5, we show the *temporal error maps*, the same metric as in [20], of two stylized consecutive frames for each method. *Ours* (bottom row) achieves the highest temporal consistency. The more high-resolution stylized sequences are available in the video.

Further details for all *shift loss* experiments: We do not compare with [19] as they require optical flow as input during testing, which is relatively expensive for our target application of real-time robotics control.

B Comparing Policy Transfer Methods: Additional Materials

Further training details for *Randomization*: As described in Sec. 4.2, each of the 8 training processes of the A3C agent renders its simulation environment with a different set of texture. Here we show the 8 different sets of textures for training the *Randomization* agent in Fig. 6.

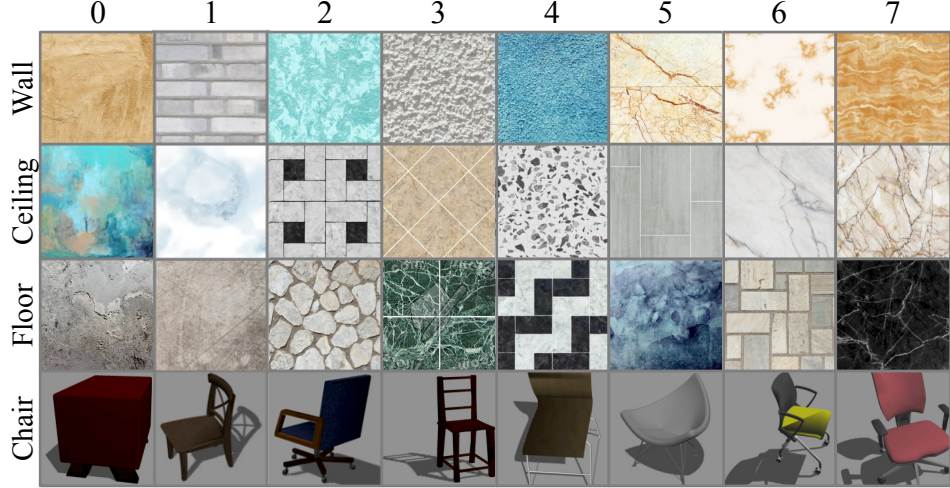


Figure 6: 8 different sets of textures for training the *Randomization* agent (Sec. 4.2).

Further implementation details for *Progressive*: We follow the same parameter initialization strategy as rin [8] for the output layers and the connection layers to guarantee that the initial policy output of the agent is identical to the first column. Observing that the simulation and real-world environments presented in [8] are relatively more visually similar than *Sim-Env* and *Real-Env1*, we additionally conduct experiments where we do not incorporate the above parameter initialization strategy, as we suspect that a random initialization might be more beneficial for transfer scenarios where two environments are more visually different. We found out that both the identical and the random initialization works, with the former converging faster. So we only report the experiments with the identical initialization, shown in the blue line in Fig. 3.

C Comparing Domain Adaptation Methods: Additional Materials

We additionally validate the *shift loss* in the field of *domain adaptation* in *outdoor* urban street scenarios (where we collect synthetic domain images $\mathbf{X} \sim p_{\text{sim}}$ from the *CARLA* simulator [28], and realistic domain images $\mathbf{Y} \sim p_{\text{real}}$ from the *RobotCar* dataset [25]). We compare the following three setups: **CyCADA** [10]: *CycleGAN* with semantic constraints, trained on single frames; **CyCADA+flow**: *CyCADA* with temporal constraints ([20]), trained on sequential frames; **Ours**: *CyCADA* with *shift loss*, trained on single frames; we refer to this as the *VR-Goggles*.

We pretrain the segmentation network $f_{\mathbf{X}}$ using *Deeplab* [11]. It is worth mentioning that the original *CyCADA* paper did not use the semantic constraint in their experiments due to memory issues. We are able to incorporate semantic loss calculation, by cropping the input images as in Sec. 4.3. The training details are also as the same as the experiments in Sec. 4.3.

In Fig. 7, we show a comparison of the subsequent frames generated by the three approaches. Our method again achieves the highest consistency and eliminates more artifacts due to the smoothness of the learned model.



Figure 7: Comparison of the translated images for sequential input frames for the different approaches. 1st row: two subsequent input frames from the realistic domain, with several representative images from the simulated domain shown in between; 2nd ~ 4th row: outputs from *CyCADA*, *CyCADA+flow* and *Ours*. Our method is able to output consistent subsequent frames and eliminate artifacts. We adjust the brightness of some zoom-ins for visualization purposes.

An additional implementation detail for all our *domain adaptation* experiments: As a naive random crop would highly likely lead to semantic permutations, we crop inputs of the two domains in the same training iteration from the same random position, and our empirical results show that this greatly stabilizes the adaptation.